ACS Photonics

Article

pubs.acs.org/journal/apchd5

Nanospectroscopic Imaging of Twinning Superlattices in an Individual GaAs-AlGaAs Core−Shell Nanowire

Alexander V. Senichev,*[,†] Vadim G. Talalaev,[†,‡] Igor V. Shtrom,[§,∥] Horst Blumtritt,[†] George E. Cirlin,[∥,⊥] Jörg Schilling,[‡] Christoph Lienau,*[,#] and Peter Werner[†]

[†]Max Planck Institute of Microstructure Physics, 06120 Halle, Germany

[‡]Martin-Luther-Universität, Centre for Innovation Competence SiLi-nano, 06120 Halle, Germany

[§]Physical Department, St. Petersburg State University, 198504 St. Petersburg, Russia

[∥]St. Petersburg Academic University RAS, 194021 St. Petersburg, Russia

[⊥]St. Petersburg State Polytechnical University, 195251 St. Petersburg, Russia

[#]Institute of Physics, Carl von Ossietzky University Oldenburg, 26129 Oldenburg, Germany

Supporting Information

ABSTRACT: GaAs nanowires (NWs) exhibit different, zinc blende (ZB) and wurzite (WZ), crystalline phases and one generally finds an uncontrolled switching between both phases on a scale of 1−10 nm. The change of crystalline structure and stacking fault density strongly affects the local confinement potential of GaAs NWs. Combining low temperature near-field spectroscopic imaging and transmission electron microscopy measurements performed on the very same individual GaAs nanowire allows us to gain an understanding of the local structure−property correlations in such wires. From the photoluminescence measurements at subwavelength spatial resolution local characteristics of the band structure are derived. In particular, our method enables us to assign the observed band gap reduction to the high level of impurity dopants and to distinguish emission from ZB-type regions and from periodically twinned superlattice regions. In this way we demonstrate the ability to trace spatial variations of the crystal structure along the wire axis by all-optical means. Our results provide direct and quantitative insight into the correlations between morphology and optics of GaAs nanowires and hence present an important step toward band gap engineering of nanowires by controlled crystal phase formation.

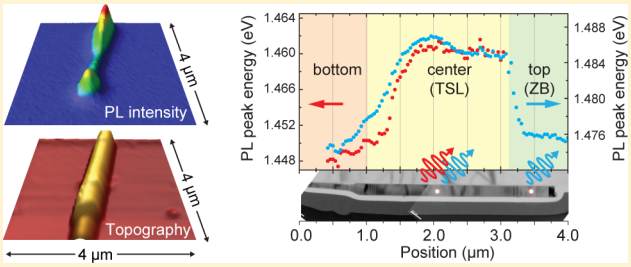

KEYWORDS: *nanospectroscopic imaging, GaAs nanowires, twinning superlattice, near-field scanning optical microscopy, transmission electron microscopy, crystal phase engineering*

The III−V based semiconductor nanowires (NWs) currently receive an upsurge of interest due to their superior optoelectronic properties as well as the compatibility with silicon technology.[1−4] These NWs are considered as promising functional building blocks for realizing advance electronic and photonic devices such as light-emitting diodes,[5] solar cells,[6] transistors,[7] or room-temperature lasers.[8] For optoelectronic applications, core−shell type nanowires have a potential advantage since the presence of a wide-bandgap shell efficiently suppresses nonradiative carrier recombination[9−11] In addition, the core−shell geometries open up possibilities for the defect-free combination of lattice-mismatched materials[12] and for tailoring the electronic band structure of radial heterostructures.[13,14]

The reliable control of the size, crystal structure, composition, and carrier concentration of such NWs as well as the fundamental studies of their structure−property relationships are essential for basically all applications of such NWs. Whereas bulk and thin film GaAs layers have a zinc blende (ZB) type equilibrium crystal structure, nanowires made of GaAs may also exhibit regions with a hexagonal, wurtzite (WZ) type crystal phase, often accompanied by stacking faults.[15−18] Experimental and theoretical findings show that the band gap of WZ GaAs is different from that of the ZB equilibrium crystal structure. Even though there is an ongoing debate about the exact value of the WZ band gap and the band gap offset between WZ and ZB GaAs, it is commonly accepted that the interfaces between both phases produce type-II band alignment with positive WZ conduction and valence band offsets.[19−25] If the controlled formation of alternating regions of ZB and WZ crystal phases in the same nanowire could be achieved, the fabrication of novel axial heterostructures with tailored own band structures would be possible. These were termed earlier "crystal phase quantum disks or dots" since the electron confinement is achieved only by the change in crystal

Received: June 6, 2014
Published: September 29, 2014

phase and not by a material change, as in usual heterostructure-defined quantum dots.[26,27]

When growing GaAs nanowires in the [111] direction, one often observes stacking fault formation and the emergence of rotational twinning in ZB type material. In such wires, ZB regions with normal ···ABCABC··· stacking sequence are followed by segments with the same ZB structure but with an atomic arrangement rotated by 180° at the twin boundary around the growth axis.[15] When observing in [1$\bar{1}$0] projection, {111}A-type lattice planes are transferred into {111}B-type lattice planes at the twin boundary, tilted with respect to each other at an angle of 141°.[28,29] These different lattice plane orientations often appear as dark and bright stripes in TEM diffraction contrast images.[15] The rotational twinning forms an ···ABCACBA··· stacking sequence[28] and the CAC stacking at the twin boundary can be considered as an inclusion of a single unit of WZ structure in a ZB matrix.

Under certain growth conditions twin planes can have a constant spacing, forming a new class of so-called twinning superlattices (TSL) and providing opportunities for electronic band structure engineering.[30] The ability to control periodic arrangements of TSL was reported for different III−V NWs.[28,29,31,32] Due to the atomically sharp interfaces of these TSL one may expect that such crystal-phase nanostructure exhibit a higher optical quality than obtained with semiconductor heterostructures of different composition. This makes TSL NWs particularly promising for device applications. So far, however, the formation of the TSL structure in GaAs NWs is mainly induced by impurity doping.[29,32] Such doping necessarily affects the optical and electronic properties and might obscure the advantages resulting from the high crystalline quality. Thus, a comprehensive study of the joint contribution of these competitive parameters to the energy band structure of TSL NWs is essential.

Future technological applications evidently require NWs with a predefined and reproducible length and sequence of WZ/ZB phases. In principle, a defined density of WZ/ZB mixture, density of stacking faults and regular arrangement of twin planes can be realized by a precise control of the growth parameters. Indeed, first successful attempts of crystal phase engineering of III−V NWs were recently reported.[28,33−36] Despite this progress, such a growth control remains a very challenging task. Moreover, it is of fundamental importance to better understand the correlation between crystalline structure and optical and electronic properties of such wires. This requires advanced characterization techniques, capable of providing a direct, high-resolution comparison of the optical and structural properties of individual nanowires. Recently, room temperature near-field PL spectra of single InP nanowires have been reported.[37] Also, various groups have focused on combining microphotoluminescence[25,26,38] and cathodoluminescence[24,25] techniques for mapping local optical spectra and transmission electron microscopy (TEM) for probing the complex morphology of III−V NWs with atomic resolution. So far, comparatively little work has been devoted to a direct correlation of optical and structural analysis performed on the very same nanowire.[22,39−41]

In this paper, we report for the first time subwavelength-resolution, low-temperature near-field photoluminescence spectra and transmission electron microscopy images of the very same GaAs-AlGaAs core−shell nanowire grown on silicon. We observe pronounced spatial variations in the emission spectrum along the length of the wire. By correlating optical and TEM analysis, we assign the emission spectra of twinning superlattice and ZB-type regions of the wire and map the local bandgap profile along the wire with a lateral resolution in the nanometer range. Our experimental approach provide possibilities for a better understanding of the interplay between morphology and optics and hence toward controlling crystal phase coexistence in such unique nanosystems.

RESULTS AND DISCUSSION

As a model system to study structure−property correlations, we used heavily beryllium-doped GaAs NWs, grown directly on a Si (111) substrate by Ga-assisted molecular beam epitaxy. Doping is essential to control the conductivity of NWs, which is necessary for the realization of optoelectronic devices.[42] Such an in situ doping strongly affects both NWs growth[43] and crystal phase formation.[29,32] In addition, photoluminescence intensities of GaAs nanostructures are generally increasing with carrier concentration, thus facilitating studies of individual NWs. Here, beryllium was taken as the most commonly used *p*-type dopant.[44] The NWs were subsequently coated with an AlGaAs shell to passivate surfaces and to enhance their emission efficiency. A side-view scanning electron microscopy (SEM) image of as-grown *p*-doped GaAs-AlGaAs core−shell NWs is presented in Figure 1a. SEM observation reveals a dense array of NWs with a typical length *L* of 2−5 μm and an average diameter of 200 nm. In comparison to site-selective growth,[9,45] the length and shapes of the NWs are nonuniform. Due to these fluctuations in wire geometry, structural and optical characterization of single NWs is particularly important. In order to isolate a single NW and to facilitate near-field scanning optical microscopy (NSOM) and TEM measurements on one and the same wire, we used ultrasonication to detach the NWs from the original substrate and then drop-coated the NWs onto a Si substrate with Au alignment marks (Figure 1b).

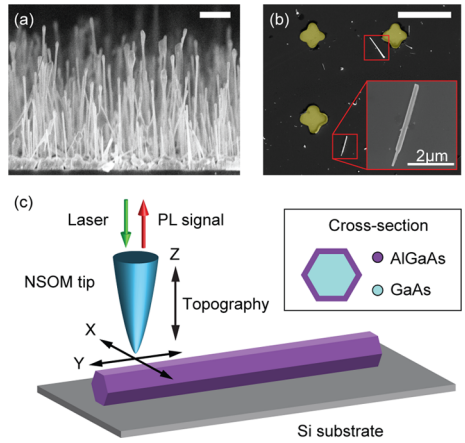

Figure 1. (a) Side-view SEM micrograph of the as-grown self-catalyzed *p*-GaAs-AlGaAs core−shell NWs on Si(111) substrate. The NWs have an average diameter of 200 nm and their length varies between 2 and 5 μm. The scale bar is 1 μm. (b) Top-view SEM micrograph of NWs transferred by ultrasonication and drop-casting techniques onto a Si substrate with Au alignment marks (yellow pseudocolor) to facilitate NSOM and TEM measurements on one and the same NW. The scale bar is 10 μm. The nanowire of interest is shown in the inset. (c) Schematic of the NSOM experiment. Local PL spectra are recorded at low temperature in illumination/collection geometry using an uncoated, chemically etched fiber probe. The inset schematically shows a cross-section of the investigated core−shell NWs.

dx.doi.org/10.1021/ph5002022 | ACS Photonics 2014, 1, 1099−1106

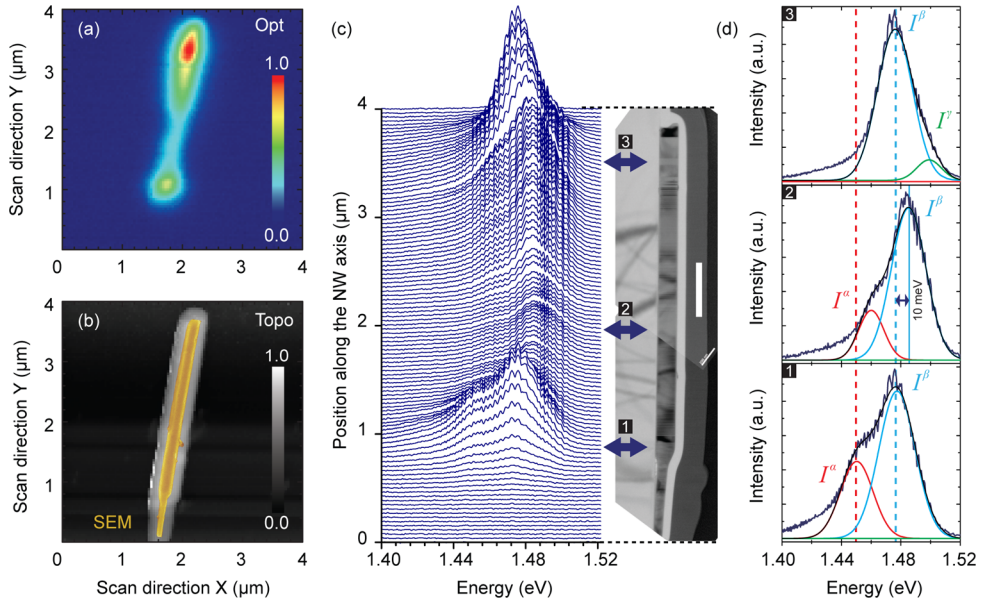

Figure 2. (a) Two-dimensional map of the total near-field PL intensity of the NW acquired at a temperature of 10 K in the region indicated by the inset in Figure 1b. A full near-field PL spectrum is recorded in the energy range between 1.245 and 1.870 eV at every pixel of the image with an integration time of 500 ms per spectrum at an estimated excitation density of ~10^2 W/cm^2. (b) Topography image recorded simultaneously during the scan process by shear force microscopy. For comparison, a SEM micrograph of the same NW, shown in yellow, is overlaid with the topography image. (c) Selected near-field PL spectra along the axis of a single NW recorded at 10 K. The right inset shows a low-resolution TEM overview of the corresponding NW. The scale bar of 500 nm applies to both the map of PL spectra along the NW axis and the TEM image, providing a direct correlation between TEM structural analysis and local near-field spectral response. (d) Selected normalized local near-field PL spectra from the regions marked by arrows in the inset of Figure 2c. The red I^{α}, blue I^{β}, and green I^{γ} lines show the decomposition of the PL spectra into three Gaussian emission bands.

Four NWs with a length of around 4 μm have been preselected for further characterization. These NWs had full contact to the Si surface and were spatially isolated from other NWs to exclude possible interactions (Figure 1b, inset).

Near-field scanning optical microscopy was used for high spatial resolution photoluminescence (PL) imaging of single NWs. The measurements were performed in a home-built low-temperature NSOM operating at 10 K inside a high vacuum chamber.[46] Low temperature measurements are helpful since the PL yield of these wires decreases substantially when increasing the temperature above 40 K and exciton ionization can become important at elevated temperatures.[20,47] All measurements were performed with HeNe laser excitation at a photon energy of 2.283 eV (543 nm). A 15 μW of laser light was coupled into an uncoated, chemically etched single mode near-field fiber probe.[48−50] The PL was collected through the same fiber in illumination/collection geometry, dispersed in an imaging monochromator and recorded with a nitrogen-cooled charge coupled device. For spatial imaging, the fiber probe was raster-scanned across the sample surface in a 4 × 4 μm^2 area with a step size of 40 nm. At every step, a full PL spectrum was recorded within an integration time of 500 ms at an estimated excitation density of ~10^2 W/cm^2. For maintaining the fiber tip in a constant and close proximity to the sample surface, a shear-force distance control method was used.[51] In this measurement configuration, we obtain a spatial resolution of about 150 nm, in agreement with earlier findings.[52] A schematic of the NSOM experiment is depicted in Figure 1c.

In Figure 2a, we present a spectrally integrated near-field photoluminescence image of the NW within a scan range of 4 × 4 μm^2. At every pixel of the image, the PL spectrum is integrated in the detection range between 1.245 and 1.870 eV and then plotted as a function of the position of the near-field probe. The topography image of this wire, simultaneously recorded during the same scan by shear force microscopy, is shown in Figure 2b. In this figure, a scanning electron microscopy (SEM) is overlaid, showing that the topography image indeed reflects the actual shape of the NW. These measurements allow us to assign the spatial origin of the different PL emission features in Figure 2a with high accuracy. Figure 2a shows two pronounced emission maxima at the top and bottom end of the NW. We verified experimentally that the decrease in PL intensity in the center region of the NW indeed is an intrinsic optical property of the wire and is not affected by distance variations between the near-field probe and the sample. Below, we will show by means of a TEM analysis that the two maxima in the near-field PL map are found in comparatively large pure ZB type regions of NW which act as carrier traps.

For a spatially resolved spectroscopic characterization, local near-field PL spectra were selected from pixels along the NW axis and plotted in Figure 2c. The PL spectra reveal a distinct spatial variation along the NW axis (a complete set of spectrally resolved 4 × 4 μm^2 maps of the PL intensity for the selected NW as well as for tree other NWs is given in the Supporting Information). Specifically, we find spectral shifts of the main emission band at around 1.48 eV along the wire axis and the emergence of new, weaker sidebands in the top and bottom regions of the wire.

Subsequent to the NSOM measurements, exactly the same NWs that have been studied optically were analyzed by transmission electron microscopy. Using focused ion beam milling a cross-section TEM sample containing the nanowire of interest was created. A set of overlapping TEM and scanning

dx.doi.org/10.1021/ph5002022 | ACS Photonics 2014, 1, 1099−1106

transmission electron microscopy (STEM) images was obtained for the entire length of the selected NWs to characterize the crystal structure with atomic resolution. Using TEM analysis supported by energy-dispersive X-ray (EDX) spatially resolved measurements we estimated a GaAs core diameter of about 134 nm and an AlGaAs shell thickness of about 23 ± 3 nm. Details of EDX measurements are presented in the Supporting Information.

A low-resolution TEM map of the NW studied by NSOM, is inset in Figure 2c with its vertical axis matched to that of the spectroscopic scan. Clearly, PL emission is suppressed in the thin region at the very bottom. This bottom part has not been passivated by an AlGaAs shell and hence the PL is quenched due to strong nonradiative recombination typical for bare GaAs NWs, in agreement with refs 10 and 11. The rest of the NW can be visually divided onto three regions, a bottom (1), center (2), and top region (3). Figure 2d shows representative PL spectra from each of these regions, marked by arrows in Figure 2c. All spectra show an intense, approximately Gaussian-shaped emission peak around 1.48 eV, labeled I^{β}, and a broad low-energy emission shoulder. In addition, the spectra in the bottom and center regions reveal a second and weaker low-energy emission band at around 1.45 eV, labeled I^{α}. Instead, those in the top region show a high-energy peak I^{γ}. As seen in Figure 2d, at energies above 1.43 eV, all near-field spectra are reasonably well described as a sum of these three Gaussian emission bands. This spectral decomposition has been performed for all the spectra in Figure 2c, providing a map of the peak energy, spectral width, and relative intensity of each of these three bands along the NW axis. A pronounced and spatially homogeneous blue shift of the I^{β} band has been observed in the central part of this specific NW. It might be interpreted as an indication for superlattice formation in this region of the NW.

To address the microscopic origin of these bands, we performed a quantitative TEM analysis of the crystal structure of the entire NW. Overlapping TEM and STEM images were analyzed to characterize the crystal structure with atomic resolution. In Figure 3, representative TEM micrographs are shown for the three wire regions selected in Figure 2c. In the depicted high-resolution STEM images each bright spot corresponds to a pair of Ga and As atoms. Distinctly different crystal structures are found in the top, center, and bottom regions of the wire. In the bottom region (Figure 3a), the conically shaped segment shows a ZB phase crystal structure with a high density of rotational twins. In the high-resolution lattice plane image, the twin interfaces are marked in red. A detailed study of the atomic stacking at the twin boundary reveals that the boundary actually represents a single monolayer (ML) of the WZ structure. Moving from the upper base to the apex of this conical segment (Figure 3a, red arrow), the density of twins gradually increases and additional larger WZ phase segments are formed at the bottom end of the NW. A similar formation of larger WZ nanodomains has also been observed in a previous study by Heiss et al.[22] The center region (Figure 3b) is of particular interest. Here, we find large rotationally twinned ZB segments with a virtually constant spacing between adjacent twin planes. This center region extends over a length of more than 2 μm. Using the atomic resolution STEM images, we counted the number of lattice planes between adjacent twin planes (Figure 3b). In the left part of this region, for positions along the NW axis of 1.0 to 1.5 μm (Figure 4b), we found a twin lattice spacing of about 19 ± 3 lattice planes per segment,

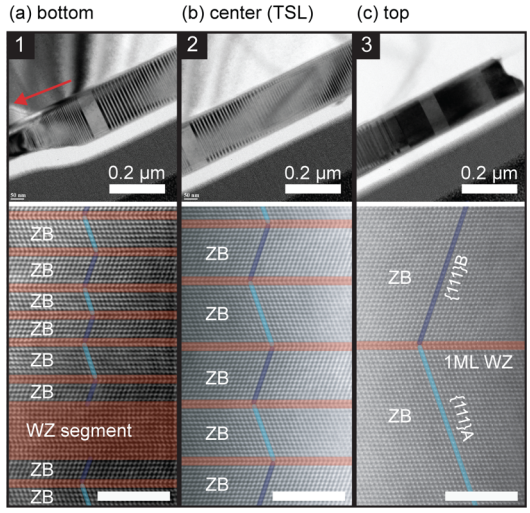

Figure 3. (Top panel) TEM micrographs of the NW from selected regions in Figure 2c together with (bottom panel) the corresponding atomic resolution STEM images showing the density and periodicity of rotational twin interfaces (in red). (a) Conically shaped bottom segment with ZB phase crystal structure, a high density of rotational twins and a larger WZ segment. This part is separated from the TSL structure by the inclusion of a 50 nm defect-free ZB segment. The red arrow indicates the direction of gradually increasing twin plane density. (b) Center segment: Large rotationally twinned ZB regions with a virtually constant spacing between adjacent twin planes forming a TSL structure that extends over more than 2 μm. (c) In the top region a ZB segment with a very low density of rotational twinning is formed. Scale bars for all STEM images are 5 nm.

corresponding to a twin density of ρ = 0.161 nm^{-1} (taking the distance between lattice planes in [111] direction as $a/(3)^{1/2}$, where a = 5.65 Å is the lattice constant of GaAs). For positions between 1.5 and 3.1 μm (Figure 4b), we find a virtually constant twin periodicity of 15 ± 3 lattice planes (ρ = 0.204 nm^{-1}). At the end of this long-range periodic TSL center region, at around 3.1 μm, there is a quite abrupt transition to the top ZB region (Figure 3c), which occurs within less than 20 nm. In Figure 4b (green circles) the linear density of twin interfaces is plotted as a function of position along the NW axis and averaged at each position over a spatial window of 150 nm, comparable to the NSOM resolution. Hence, the structural analysis reveals a more than 2 μm long TSL region with an almost perfectly homogeneous spacing between adjacent twin planes. This TSL region is surrounded by two ZB segments, one at the bottom with a high density of twin defects (Figure 3a) and one at the top with a very low density of twin planes (Figure 3c). So far, such clear indications of TSL formation have only been observed for this specific NW which makes it particularly attractive for an in-depth investigation of correlations between its crystal structure and optical properties.

This structural characterization now allows for the assignment of the local optical spectra reported in Figure 2. We start with an analysis of the top region. Here, the emission is dominated by the I^{β} band. Its emission peak with a width of about 26 meV (full width at half-maximum, fwhm) is centered at 1.476 eV, independent of the exact position along the wire axis for this region. The I^{α} emission is suppressed and a characteristic high energy shoulder I^{γ} is found in the spectra (Figure 2d). Such emission spectra are characteristic for heavily p-doped ZB type GaAs.[53,54] The main emission, I^{β}, reflects direct, **k**-conserving optical transitions between the minimum

dx.doi.org/10.1021/ph5002022 | ACS Photonics 2014, 1, 1099−1106

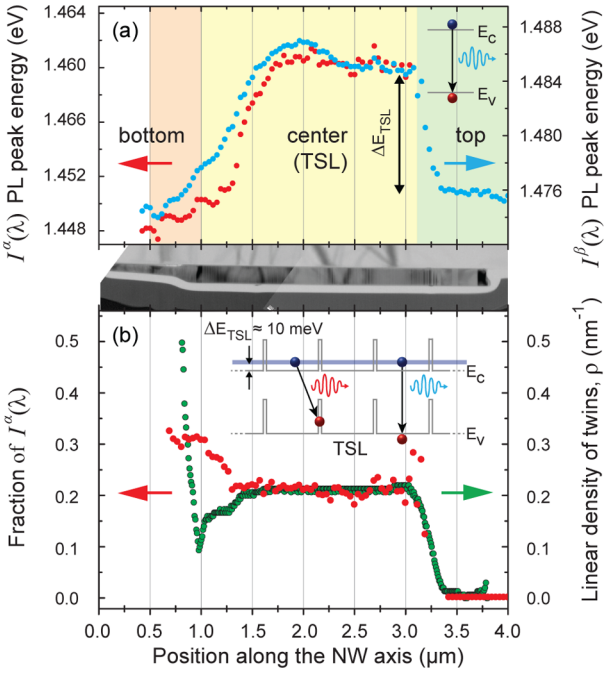

Figure 4. (a) Spatial variation of the peak energies of the I^α (red circles) and I^β (blue circles) emission peaks along the nanowire axis. Inset: Schematic of the ZB GaAs band-to-band transition giving rise to the I^β emission in the top region. (b) Relative fraction of the I^α emission to the total PL emission in different parts of the NW (red circles) and variation of the linear density of twin planes along the NW axis (green circles). The twin density is spatially averaged over 150 nm, comparable to the NSOM resolution. Inset: Schematic of the origin of the I^α (red) and I^β (blue) emission in the center TSL region of the NW.

of the conduction band and the top of the valence band (see inset in Figure 4a). The high energy shoulder, I^γ, originates from indirect, non-**k**-conserving transitions into holes states near the valence band quasi-Fermi level.[53,54]

The peak energy of the I^β emission is clearly red-shifted with respect to the band gap of ZB-type bulk GaAs. This reflects a band gap shrinkage in *p*-doped GaAs due to exchange and correlation in the hole system,[53] scaling with the third root of the hole concentration. Following ref 53, we estimate a band gap shrinkage of 68 meV from the PL spectrum in Figure 2d (top region). This points to a local hole concentration of about 8×10^{19} cm^{-3}. This agrees well with the chosen in situ doping level for the studied NWs which was set to $\sim 5 \times 10^{19}$ cm^{-3}.

We have therefore tried to map the local Beryllium doping level by means of energy-dispersive X-ray (EDX) spectroscopy and electron energy loss spectroscopy (EELS) measurements (see Supporting Information). The doping level in our NWs, however, was below the sensitivity limit of these techniques. Large clusters with high Beryllium concentration would have been resolved in these measurements. Since we did not find such precipitates, we conclude that Beryllium is substitutionally incorporated in our NWs. More detailed information about the local Beryllium doping can be extracted from the near-field PL spectra. Near-field PL spectra of a reference, Be-doped NW from the same growth run with a defect-free ZB crystal structure are shown in the Supporting Information. The spectra are very similar to those recorded in the top region of the present NW. In the pure ZB Be-doped NW, I^β and I^γ emission bands are also observed. The I^β band is centered at ~1.475 eV and has a width of about 25 meV (fwhm). This agrees reasonably well with literature results on heavily *p*-doped GaAs for doping levels of $\sim 5 \times 10^{19}$ cm^{-3}, showing an average band gap shrinkage to ~1.460 eV at 10 K,[53] a corresponding red shift of the PL peak[55] and a broadening of the emission lines to a width of about 19 meV.[56,57]

The spatially homogeneous peak energy and bandwidth in the top region of Figure 2 is thus taken as an indication for a spatially homogeneous doping profile in this nanowire. This is supported by recent growth studies,[58] showing that pronounced changes in growth temperature are needed to induce pronounced gradients in doping concentration. We therefore conclude that the doping in our nanowire is spatially rather homogeneous. As such, spatial variations of the optical properties, such as the emergence of the new optical bands, are likely to reflect changes in the local crystal structure, unless the bandwidth of the optical band is changed substantially.

We now turn to the spectra recorded in the bottom region of the wire, at positions between 0.5 and 1.0 μm. Evidently, these spectra are more complex. Here, we find a strong low-energy emission peak, I^α, red-shifted by about 26 meV with respect to the I^β emission. This low energy emission is seen in all regions with a sufficiently high density of twin defects and hence is clearly related to the presence of these defects. In particular, the I^α band is absent in the ZB reference NW with similar doping level. Its line width (~25 meV) does not change much with position along the NW. Since we do not see a significant change in line width, we assume that the local beryllium doping concentration, which is the main cause for the line broadening, is spatially rather homogeneous along the NW. All the arguments point to an assignment of the I^α band to a spatially indirect emission between electron states in the conduction band of ZB GaAs and a confined hole state in the WZ layer at the twin interface.[27,59]

Its red shift with respect to the I^β emission of about 26 meV then provides a measure of the hole confinement energy at inclusions of WZ unit cells in a ZB matrix. The magnitude of this red shift changes slightly (by about 3 meV) with position and thus with twin defect density (Figure 4a). These observed shifts are considerably larger than the binding energy of an exciton at a single twin defect (~5 meV).[59] Reasonable estimates of the shifts can be obtained from recently introduced superlattice models for the lowest PL transition energy.[22] In the bottom region of the NW, the relative amplitude of the I^α is quite large (Figure 4b, red circles). The peak energy of the I^β emission is similar to that in the top region of the NW, even though the density of twin interfaces increases substantially from 1.0 to 0.5 μm (Figure 4b). This may also point to a quantum confinement of electronic states but it is difficult to clearly assign the quantum confinement effects on the local optical spectra in the bottom part of the NW. In this region, it is challenging to clearly correlate structural and optical properties of the NW for a variety of reasons: (i) larger segments of WZ phase are formed, apparently red-shifting the optical spectra, (ii) the dopant level may be different from that in the top region and vary with position, (iii) the thickness of the AlGaAs shell surrounding the NW is varying, affecting the optical resonance energies and emission intensities, and (iv) the crystal structure varies on a scale that is small compared to the optical resolution and the carrier diffusion length, and hence, such correlations may not be fully resolved in the present experiments.

dx.doi.org/10.1021/ph5002022 | ACS Photonics 2014, 1, 1099−1106

Evidence for electron quantization in twin plane superlattices is found, however, in the center region of the nanowire, at positions between 1.0 and 3.1 μm. Throughout this region, we find a significant contribution from the I^{α} band (Figure 4a). Moving from the topmost ZB-type region of the NW to TSL structure, we observe, in parallel with the emergence of the I^{α} band, an abrupt blue shift of the I^{β} peak by about $\Delta E_{TSL} \approx 10$ meV in the region from 3.3 to 3.1 μm. Since we assume a nearly homogeneous doping level along the NW growth direction, we describe the PL spectral behavior in the TSL region as a function of the crystal structure variation only. The abrupt shift of the I^{β} peak energy at the interface between pure ZB-type segment and TSL structure supports this approach (Figure 4a).

Theoretical calculations suggest that the TSL structure gives rise to electron quantum confinement in the ZB phase and miniband formation, with miniband energies varying with twin density.[60] The thin barriers formed by the WZ monolayers allow for efficient electron tunneling between adjacent ZB type regions and, hence, electron delocalization and superlattice formation.[60] In this TSL center region, the dominant I^{β} peak is then assigned to a transition between the lowest TSL conduction miniband and a valence band hole state in the ZB region of the TSL (see inset in Figure 4b, blue photon). The I^{α} emission on the other hand reflects transitions between TSL states and heavy-hole-like bound states in WZ monolayers (see inset in Figure 4b, red photon). The energy splitting between both bands is position independent for this region. The variation in peak energy of both the I^{α} and I^{β} peaks with twin density tracks the spatial variation in quantum confinement of the delocalized electron states. Here, both the structural TEM characterization and our optical data give evidence for the formation of a spatially highly homogeneous twinning superlattice region with delocalized electron states, with wave functions extending through the superlattice.

The formation of these twin plane superlattices and the resulting conduction miniband now could also explain the strong emission intensities seen at the edges of the NW in Figure 2a. In these outer top and bottom regions, electron quantization is reduced, minibands do not exist due to the lacking periodicity of ZB and WZ regions and the electron states are more similar to those of a planar ZB region. Hence, electrons created in high-energy conduction band states of the TSL region will drift-diffuse into lower energy conduction band states in the outer region, acting as efficient electron traps. As seen in the optical spectra in Figure 2b, the emission intensity in the center TSL region is therefore reduced and greatly enhanced emission intensity is observed at the very ends of the nanowire.

SUMMARY AND CONCLUSIONS

In summary, we have combined low temperature near-field scanning optical microscopy and high-resolution electron microscopy measurements to explore the correlation between crystal structure and local optical properties of a single *p*-doped GaAs-AlGaAs core−shell nanowire. Our measurements provide a direct reconstruction of the local optical band gap profile with 150 nm spatial resolution and reveal a distinct local variation in the optical spectra along the wire axis, induced by changes of the local crystalline structure of the NW. Together, TEM and NSOM experiments provide evidence for hole localization in a monolayer of wurtzite type GaAs at the interface between two rotationally twinned ZB segments. More importantly, our data strongly suggest electron quantum confinement in the conduction band of a periodic twinning superlattice array. Throughout a mesoscopic range of more than 1.5 μm, this TSL array shows a virtually perfect periodic arrangement of the twin interfaces. The observed blue-shifts of the local PL spectra are qualitatively explained in terms of quantum confinement model suggesting miniband formation and electron delocalization in the TSL conduction band. At present, the resulting optical spectra are largely inhomogeneously broadened due to the presence of a comparatively high level of beryllium dopants. This calls for studies of nanowires with reduced dopant levels in order to unveil the positive effects of the intrinsically high structural quality of the twin interfaces on their optical properties. Our results also suggest that it may be of substantial interest to explore the drift-diffusive carrier transport in this class of nanowires. Such experiments are currently underway in our laboratories.

METHODS

Nanowire Growth. The investigated core−shell GaAs-AlGaAs nanowires were grown by a commercial molecular beam epitaxy system EP-1203. Before the growth of NWs, the Si(111) substrate was annealed in vacuum at 660 °C in order to partially desorb the oxide layer. After the temperature has decreased to 610 °C, a flux of Ga was supplied to the surface for 60 s to create catalyst nanoparticles. Then, an As flux was opened to initiate the growth of GaAs NWs. The As_4/Ga fluxes ratio and the deposition rate were held at 0.5 and 1 ML/s, respectively. The temperature of the Be-source cell was set to 860 °C, which corresponds to a doping level of $\sim 5 \times 10^{19}$ cm^{-3} for the case of planar GaAs layers grown on a GaAs(111)B (determined by Van der Pauw measurements). The total growth time of a GaAs segment was 15 min. After the growth was interrupted, the temperature of the sample was reduced to 550 °C and the $Al_{0.3}Ga_{0.7}As$ shell was grown within 5 min. The NWs grown by such a Ga-assisted technique have typically predominantly ZB crystal structure.[61,62]

Si Substrate with Alignment Marks. A Si substrate was chosen because, in contrast to TEM holey carbon-coated Cu grids, the Si flat surface ensures a stable contact of the NW with the substrate and a good thermal dissipation during NSOM measurements. Several alignment marks were placed onto the Si substrate before dispersing GaAs NWs. Large scale SEM images were then used to select four nanowires, randomly distributed on the substrate, for TEM and NSOM measurements.

Near-Field Scanning Optical Microscopy. For high spatial resolution imaging of single NW photoluminescence, we used a low-temperature near-field scanning optical microscope operating at a temperature of 10 K inside a high vacuum chamber.[46] All measurements were performed in near-field illumination-collection mode,[52] using an uncoated, chemically etched single mode fiber as near-field probe.[48−50] Such uncoated near-field fiber probes combine a spatial optical resolution of about $\lambda/4$ to $\lambda/6$ with a high collection efficiency and minimum perturbation of the optical properties of the semiconductor nanostructure. For optical excitation, we coupled 15 μW of light from a helium−neon laser at a photon energy of 2.283 eV (543 nm) into the near-field fiber probe. The PL signal was collected through the same fiber probe (Figure 1c), dispersed in an imaging monochromator, and detected with a nitrogen-cooled charge-coupled device camera.

Transmission Electron Microscopy. A focused ion beam (FIB) target preparation technique was applied to prepare the

dx.doi.org/10.1021/ph5002022 | ACS Photonics 2014, 1, 1099−1106

TEM sample including the NW of interest. At first, the selected NW was covered by carbon and platinum layers to protect the structure during the FIB milling. Then, a piece with a size of 8.5 × 3.0 × 8.0 μm^3, containing protection layers, the NW, and a part of Si substrate, was cut out by FIB and transferred on a TEM holder with the help of a needle-shaped micromanipulator. Finally, this slice was thinned by ion-milling down to a thickness of about 80 nm in correspondence with the NW diameter. The morphology and crystal structure of the NW were then analyzed by TEM and STEM in a FEI microscope TITAN 80−300, which was probe-corrected to receive a point-to point resolution of about 1 Å. The measurements of the lattice structure were performed in ⟨110⟩ orientation in which the stacking sequence of consecutive {111} layers could be determined.

■ ASSOCIATED CONTENT

Supporting Information

Video files showing a complete set of spectrally resolved 4 × 4 μm^2 near-field PL maps of four different nanowires, characteristic PL spectra of the reference heavily beryllium-doped GaAs nanowire with a defect-free ZB crystal structure, and EDX and EELS measurements of a single nanowire. This material is available free of charge via the Internet at http://pubs.acs.org.

■ AUTHOR INFORMATION

Corresponding Authors

*E-mail: senichev@mpi-halle.mpg.de.
*E-mail: christoph.lienau@uni-oldenburg.de.

Notes

The authors declare no competing financial interest.

■ ACKNOWLEDGMENTS

This research was performed within the International Max Planck Research School for Science and Technology of Nanostructures. A.V.S. thanks O. Brovko for valuable discussions and E. Pippel for EDX and EELS measurements. I.V.S. acknowledges financial support by the Russian foundation for basic research and Scientific Grants for St. Petersburg State University. The nanowire samples were grown under the support of Russian Science Foundation (Project No 14-12-00393). C.L. wishes to gratefully acknowledge financial support by the Deutsche Forschungsgemeinschaft (SPP1391), the European Union (CRONOS), and the Korea Foundation for International Cooperation of Science and Technology (Global Research Laboratory Project, K20815000003). V.G.T. and J.S. acknowledge financial support by the German Ministry of Education and Research for the Centre for Innovation Competence SiLi-nano (project number 03Z2HN12).

■ REFERENCES

(1) Yang, P.; Yan, R.; Fardy, M. Semiconductor nanowire: what's next? *Nano Lett.* **2010**, *10*, 1529−1536.

(2) Bjork, M. T.; Schmid, H.; Bessire, C. D.; Moselund, K. E.; Ghoneim, H.; Karg, S.; Lortscher, E.; Riel, H. Si−InAs heterojunction Esaki tunnel diodes with high current densities. *Appl. Phys. Lett.* **2010**, *97*, 163501.

(3) Tomioka, K.; Tanaka, T.; Hara, S.; Hiruma, K.; Fukui, T. III-V nanowires on Si substrate: Selective-area growth and device applications. *IEEE J. Sel. Top. Quantum Electron.* **2011**, *17*, 1112−1129.

(4) Hocevar, M.; Immink, G.; Verheijen, M.; Akopian, N.; Zwiller, V.; Kouwenhoven, L.; Bakkers, E. Growth and optical properties of axial hybrid III−V/silicon nanowires. *Nat. Commun.* **2012**, *3*, 1266.

(5) Tomioka, K.; Motohisa, J.; Hara, S.; Hiruma, K.; Fukui, T. GaAs/AlGaAs core multishell nanowire-based light-emitting diodes on Si. *Nano Lett.* **2010**, *10*, 1639−1644.

(6) Hu, S.; Chi, C.-Y.; Fountaine, K. T.; Yao, M.; Atwater, H. A.; Dapkus, P. D.; Lewis, N. S.; Zhou, C. Optical, electrical, and solar energy-conversion properties of gallium arsenide nanowire-array photoanodes. *Energy Environ. Sci.* **2013**, *6*, 1879−1890.

(7) Tomioka, K.; Yoshimura, M.; Fukui, T. A III−V nanowire channel on silicon for high-performance vertical transistors. *Nature* **2012**, *488*, 189−192.

(8) Wang, Z.; Tian, B.; Paladugu, M.; Pantouvaki, M.; Le Thomas, N.; Merckling, C.; Guo, W.; Dekoster, J.; Van Campenhout, J.; Absil, P.; Van Thourhout, D. Polytypic InP nanolaser monolithically integrated on (001) silicon. *Nano Lett.* **2013**, *13*, 5063−5069.

(9) Tomioka, K.; Kobayashi, Y.; Motohisa, J.; Hara, S.; Fukui, T. Selective-area growth of vertically aligned GaAs and GaAs/AlGaAs core-shell nanowires on Si(111) substrate. *Nanotechnology* **2009**, *20*, 145302.

(10) Sköld, N.; Karlsson, L. S.; Larsson, M. W.; Pistol, M.-E.; Seifert, W.; Trägårdh, J.; Samuelson, L. Growth and optical properties of strained GaAs−Ga(x)In(1 − x)P core-shell nanowires. *Nano Lett.* **2005**, *5*, 1943−1947.

(11) Titova, L. V.; Hoang, T. B.; Jackson, H. E.; Smith, L. M.; Yarrison-Rice, J. M.; Kim, Y.; Joyce, H. J.; Tan, H. H.; Jagadish, C. Temperature dependence of photoluminescence from single core-shell GaAs-AlGaAs nanowires. *Appl. Phys. Lett.* **2006**, *89*, 173126.

(12) Durand, C.; Bougerol, C.; Carlin, J.-F.; Rossbach, G.; Godel, F.; Eymery, J.; Jouneau, P.-H.; Mukhtarova, A.; Butté, R.; Grandjean, N. M-plane GaN/InAlN multiple quantum wells in core-shell wire structure for UV emission. *ACS Photonics* **2014**, *1*, 38−46.

(13) Dimakis, E.; Jahn, U.; Ramsteiner, M.; Tahraoui, A.; Grandal, J.; Kong, X.; Marquardt, O.; Trampert, A.; Riechert, H.; Geelhaar, L. Coaxial multishell (In,Ga)As/GaAs nanowires for near-infrared emission on Si substrates. *Nano Lett.* **2014**, *14*, 2604−2609.

(14) Weiss, M.; Kinzel, J. B.; Schülein, F. J. R.; Heigl, M.; Rudolph, D.; Morkötter, S.; Döblinger, M.; Bichler, M.; Abstreiter, G.; Finley, J. J.; Koblmüller, G.; Wixforth, A.; Krenner, H. J. Dynamic acoustic control of individual optically active quantum dot-like emission centers in heterostructure nanowires. *Nano Lett.* **2014**, *14*, 2256−2264.

(15) Koguchi, M.; Kakibayashi, H.; Yazawa, M.; Hiruma, K.; Katsuyama, T. Crystal structure change of GaAs and InAs whiskers from zinc-blende to Wurtzite type. *Jpn. J. Appl. Phys.* **1992**, *31*, 2061−2065.

(16) Hiruma, K.; Yazawa, M.; Katsuyama, T.; Ogawa, K.; Haraguchi, K.; Koguchi, M.; Kakibayashi, H. Growth and optical properties of nanometer-scale GaAs and InAs whiskers. *J. Appl. Phys.* **1995**, *77*, 447−462.

(17) Persson, A. I.; Larsson, M. W.; Stenström, S.; Ohlsson, B. J.; Samuelson, L.; Wallenberg, L. R. Solid-phase diffusion mechanism for GaAs nanowire growth. *Nat. Mater.* **2004**, *3*, 677−681.

(18) Harmand, J. C.; Patriarche, G.; Pere-Laperne, N.; Merat-Combes, M.-N.; Travers, L.; Glas, F. Analysis of vapor-liquid-solid mechanism in Au-assisted GaAs nanowire growth. *Appl. Phys. Lett.* **2005**, *87*, 203101.

(19) Murayama, M.; Nakayama, T. Chemical trend of band offsets at wurtzite/zinc-blende heterocrystalline semiconductor interfaces. *Phys. Rev. B* **1994**, *49*, 4710−4724.

(20) Hoang, T. B.; Moses, A. F.; Zhou, H. L.; Dheeraj, D. L.; Fimland, B. O.; Weman, H. Observation of free exciton photoluminescence emission from single wurtzite GaAs nanowires. *Appl. Phys. Lett.* **2009**, *94*, 133105.

(21) De, A.; Pryor, C. E. Predicted band structures of III−V semiconductors in the wurtzite phase. *Phys. Rev. B* **2010**, *81*, 155210.

(22) Heiss, M.; Conesa-Boj, S.; Ren, J.; Tseng, H.-H.; Gali, A.; Rudolph, A.; Uccelli, E.; Peiró, F.; Morante, J. R.; Schuh, D.; Reiger, E.; Kaxiras, E.; Arbiol, J.; Fontcuberta i Morral, A. Direct correlation of crystal structure and optical properties in wurtzite/zinc-blende GaAs nanowire heterostructures. *Phys. Rev. B* **2011**, *83*, 045303.

(23) Ketterer, B.; Heiss, M.; Livrozet, M. J.; Rudolph, A.; Reiger, E.; Fontcuberta i Morral, A. Determination of the band gap and the split-off band in wurtzite GaAs using Raman and photoluminescence excitation spectroscopy. *Phys. Rev. B* **2011**, *83*, 125307.
(24) Jahn, U.; Lähnemann, J.; Pfüller, C.; Brandt, O.; Breuer, S.; Jenichen, B.; Ramsteiner, M.; Geelhaar, L.; Riechert, H. Luminescence of GaAs nanowires consisting of wurtzite and zinc-blende segments. *Phys. Rev. B* **2012**, *85*, 045323.
(25) Spirkoska, D.; et al. Structural and optical properties of high quality zinc-blende/wurtzite GaAs nanowire heterostructures. *Phys. Rev. B* **2009**, *80*, 245325.
(26) Akopian, N.; Patriarche, G.; Liu, L.; Harmand, J.-C.; Zwiller, V. Crystal phase quantum dots. *Nano Lett.* **2010**, *10*, 1198−1201.
(27) Corfdir, P.; Van Hattem, B.; Uccelli, E.; Conesa-Boj, S.; Lefebvre, P.; Fontcuberta I Morral, A.; Phillips, R. T. Three-dimensional magneto-photoluminescence as a probe of the electronic properties of crystal-phase quantum disks in GaAs nanowires. *Nano Lett.* **2013**, *13*, 5303−5310.
(28) Caroff, P.; Dick, K. A.; Johansson, J.; Messing, M. E.; Deppert, K.; Samuelson, L. Controlled polytypic and twin-plane superlattices in III−V nanowires. *Nat. Nanotechnol.* **2009**, *4*, 50−55.
(29) Burgess, T.; Breuer, S.; Caroff, P.; Wong-Leung, J.; Gao, Q.; Hoe Tan, H.; Jagadish, C. Twinning superlattice formation in GaAs nanowires. *ACS Nano* **2013**, *7*, 8105−8114.
(30) Ikonic, Z.; Srivastava, G.; Inkson, J. Optical properties of twinning superlattices in diamond-type and zinc-blende-type semiconductors. *Phys. Rev. B* **1995**, *52*, 14078−14085.
(31) Algra, R. E.; Verheijen, M. A.; Borgström, M. T.; Feiner, L.-F.; Immink, G.; van Enckevort, W. J. P.; Vlieg, E.; Bakkers, E. P. A. M. Twinning superlattices in indium phosphide nanowires. *Nature* **2008**, *456*, 369−372.
(32) Dowdy, R.; Mohseni, P.; Fortuna, S. A.; Wen, J.; Li, X. Twinning Superlattice in VLS Grown Planar GaAs Nanowires Induced by Impurity Doping. IEEE Photonics Conf., New York, NY, Dec 10, 2012, IEEE: New York, NY, 2012; pp 693−694.
(33) Dick, K. A.; Thelander, C.; Samuelson, L.; Caroff, P. Crystal phase engineering in single InAs nanowires. *Nano Lett.* **2010**, *10*, 3494−3499.
(34) Rieger, T.; Lepsa, M. I.; Schäpers, T.; Grützmacher, D. Controlled wurtzite inclusions in self-catalyzed zinc blende III−V semiconductor nanowires. *J. Cryst. Growth* **2013**, *378*, 506−510.
(35) Dheeraj, D. L.; Munshi, A. M.; Scheffler, M.; van Helvoort, A. T. J.; Weman, H.; Fimland, B. O. Controlling crystal phases in GaAs nanowires grown by Au-assisted molecular beam epitaxy. *Nanotechnology* **2013**, *24*, 015601.
(36) Munshi, A. M.; Dheeraj, D. L.; Todorovic, J.; van Helvoort, A. T.; Weman, H.; Fimland, B. r.-O. Crystal phase engineering in self-catalyzed GaAs and GaAs/GaAsSb nanowires grown on Si(111). *J. Cryst. Growth* **2013**, *372*, 163−169.
(37) Bao, W.; et al. Mapping local charge recombination heterogeneity by multidimensional nanospectroscopic imaging. *Science* **2012**, *338*, 1317−1321.
(38) Spirkoska, D.; Efros, A. L.; Lambrecht, W. R. L.; Cheiwchanchamnangij, T.; Fontcuberta i Morral, A.; Abstreiter, G. Valence band structure of polytypic zinc-blende/wurtzite GaAs nanowires probed by polarization-dependent photoluminescence. *Phys. Rev. B* **2012**, *85*, 045309.
(39) Bao, J.; Bell, D. C.; Capasso, F.; Wagner, J. B.; Mårtensson, T.; Trägårdh, J.; Samuelson, L. Optical properties of rotationally twinned InP nanowire heterostructures. *Nano Lett.* **2008**, *8*, 836−841.
(40) Todorovic, J.; Moses, A. F.; Karlberg, T.; Olk, P.; Dheeraj, D. L.; Fimland, B. O.; Weman, H.; van Helvoort, A. T. J. Correlated micro-photoluminescence and electron microscopy studies of the same individual heterostructured semiconductor nanowires. *Nanotechnology* **2011**, *22*, 325707.
(41) Ahtapodov, L.; Todorovic, J.; Olk, P.; Mjåland, T.; Slåttnes, P.; Dheeraj, D. L.; van Helvoort, A. T. J.; Fimland, B. r.-O.; Weman, H. A story told by a single nanowire: optical properties of wurtzite GaAs. *Nano Lett.* **2012**, *12*, 6090−6095.
(42) Wallentin, J.; Borgström, M. T. Doping of semiconductor nanowires. *J. Mater. Res.* **2011**, *26*, 2142−2156.
(43) Yee, R. J.; Gibson, S. J.; Dubrovskii, V. G.; LaPierre, R. R. Effects of Be doping on InP nanowire growth mechanisms. *Appl. Phys. Lett.* **2012**, *101*, 263106.
(44) Ploog, K. The use of Si and Be impurities for novel periodic doping structures in GaAs grown by molecular beam epitaxy. *J. Electrochem. Soc.* **1981**, *128*, 400−410.
(45) Fan, H. J.; Werner, P.; Zacharias, M. Semiconductor nanowires: from self-organization to patterned growth. *Small* **2006**, *2*, 700−717.
(46) Behme, G.; Richter, A.; Suptitz, M.; Lienau, C. Vacuum near-field scanning optical microscope for variable cryogenic temperatures. *Rev. Sci. Instrum.* **1997**, *68*, 3458−3463.
(47) Graham, A. M.; Corfdir, P.; Heiss, M.; Conesa-Boj, S.; Uccelli, E.; Fontcuberta i Morral, A.; Phillips, R. T. Exciton localization mechanisms in wurtzite/zinc-blende GaAs nanowires. *Phys. Rev. B* **2013**, *87*, 125304.
(48) Intonti, F.; Emiliani, V.; Lienau, C.; Elsaesser, T.; Savona, V.; Runge, E.; Zimmermann, R.; Nötzel, R.; Ploog, K. Quantum mechanical repulsion of exciton levels in a disordered quantum well. *Phys. Rev. Lett.* **2001**, *87*, 076801.
(49) Emiliani, V.; Guenther, T.; Lienau, C.; Nötzel, R.; Ploog, K. Ultrafast near-field spectroscopy of quasi-one-dimensional transport in a single quantum wire. *Phys. Rev. B* **2000**, *61*, 10583−10586.
(50) Guenther, T.; Lienau, C.; Elsaesser, T.; Glanemann, M.; Axt, V.; Kuhn, T.; Eshlaghi, S.; Wieck, A. Coherent nonlinear optical response of single quantum dots studied by ultrafast near-field spectroscopy. *Phys. Rev. Lett.* **2002**, *89*, 057401.
(51) Karrai, K.; Grober, R. D. Piezoelectric tip-sample distance control for near field optical microscopes. *Appl. Phys. Lett.* **1995**, *66*, 1842−1844.
(52) Intonti, F.; Emiliani, V.; Lienau, C.; Elsaesser, T.; Nötzel, R.; Ploog, K. Near-field optical spectroscopy of localized and delocalized excitons in a single GaAs quantum wire. *Phys. Rev. B* **2001**, *63*, 075313.
(53) Olego, D.; Cardona, M. Photoluminescence in heavily doped GaAs. I. Temperature and hole-concentration dependence. *Phys. Rev. B* **1980**, *22*, 886−893.
(54) Nagle, J.; Malik, R.; Gershoni, D. A comparison of atomic carbon versus beryllium acceptor doping in GaAs grown by molecular beam epitaxy. *J. Cryst. Growth* **1991**, *111*, 264−268.
(55) Zhang, D.; Radhakrishnan, K.; Yoon, S.; Han, Z. Photoluminescence in degenerate p-type GaAs layers grown by molecular beam epitaxy. *Mater. Sci. Eng., B* **1995**, *35*, 449−453.
(56) Kim, S.-I.; Kim, M.-S.; Kim, Y.; Eom, K. S.; Min, S.-K.; Lee, C. Low temperature photoluminescence characteristics of carbon doped GaAs. *J. Appl. Phys.* **1993**, *73*, 4703−4705.
(57) Zhang, D.; Radhakrishnan, K.; Yoon, S. Characterization of beryllium-doped molecular beam epitaxial grown GaAs by photoluminescence. *J. Cryst. Growth* **1995**, *148*, 35−40.
(58) Korte, S.; Steidl, M.; Prost, W.; Cherepanov, V.; Voigtlander, B.; Zhao, W.; Kleinschmidt, P.; Hannappel, T. Resistance and dopant profiling along freestanding GaAs nanowires. *Appl. Phys. Lett.* **2013**, *103*, 143104.
(59) Rudolph, D.; Schweickert, L.; Morkötter, S.; Hanschke, L.; Hertenberger, S.; Bichler, M.; Koblmüller, G.; Abstreiter, G.; Finley, J. J. Probing the trapping and thermal activation dynamics of excitons at single twin defects in GaAsAlGaAs core shell nanowires. *New J. Phys.* **2013**, *15*, 113032.
(60) Ikonić, Z.; Srivastava, G.; Inkson, J. Electronic properties of twin boundaries and twinning superlattices in diamond-type and zinc-blende-type semiconductors. *Phys. Rev. B* **1993**, *48*, 17181−17193.
(61) Cirlin, G. E.; Dubrovskii, V. G.; Samsonenko, Y. B.; Bouravleuv, A. D.; Durose, K.; Proskuryakov, Y. Y.; Mendes, B.; Bowen, L.; Kaliteevski, M. A.; Abram, R. A.; Zeze, D. Self-catalyzed, pure zincblende GaAs nanowires grown on Si(111) by molecular beam epitaxy. *Phys. Rev. B* **2010**, *82*, 035302.
(62) Dubrovskii, V. G.; Cirlin, G. E.; Sibirev, N. V.; Jabeen, F.; Harmand, J. C.; Werner, P. New mode of vapor-liquid-solid nanowire growth. *Nano Lett.* **2011**, *11*, 1247−1253.